RC1:

This study characterizes NPF in a coastal city in China and discusses the NPF contribution to CCN concentration. There is an in depth comparison of how NPF events differ from non-NPF days in terms of the aerosol size distribution, chemical composition/hygroscopicity, and precursor gases. I thought the authors did a good job of discussing their results and explaining how different mechanisms contribute to formation and growth of NPF. My comments are mostly about clarification/the need for additional details about the methods.

Response: We appreciate the time and effort that the editor and the reviewers dedicated to providing feedback on our manuscript. We are grateful for the insightful comments and valuable improvements to our paper. We have incorporated most of the suggestions made by the reviewers. According to your suggestion, we modified the manuscript in detail and marked the revised contents with red font.

Major Comments

1. I would suggest reframing the goal in the (introduction) and outcome (conclusion) of this study away from wording such as "quantification of its ultimate climate effects" (Line 76) and "climatic impact of NPF" (Line 392). While this study does quantify and discuss mechanisms of NPF and their contribution to CCN concentrations, it may be more precise to frame this work as defining the CCN efficiency or cloud nucleating ability of NPF, or the *potential* climatic impact of NPF. Better understanding and representing CCN concentration is an important bridge to understanding their climate effects, but an actual cloud impact due to CCN is not quantified in the paper.

- On this note, it would also be helpful to state more directly at the end of the introduction the primary new aspect of the work. Is it new/unique because of the region specifically? Because of the focus on linking observations to the various mechanisms? Initially it read to me like the unique aspect was linking NPF to CCN, which the authors recognize in Lines 64-70 has been done in other studies.

Response: We thank the reviewer for this thoughtful and constructive comment. We fully agree that our original wording overstated the direct climate relevance of our findings, and that the novelty of the work was not clearly distinguished from previous studies that have already linked NPF events to increased CCN concentrations. we have made the following revisions:

Line 93-96: However, some studies suggest that an increase in hydrophobic organic components during subsequent particle growth may inhibit CCN generation. Therefore, understanding the role of different components during particle growth is crucial for assessing their subsequent climate effects.

Line 101-104: Currently, understanding how regional variations in atmospheric oxidants and precursors affect the growth of newly formed particles to CCN sizes, especially the quantification of their CCN efficiency, remains a challenge and a frontier in current research.

Line 529-530: This work demonstrates that the potential climatic impact of NPF in coastal urban areas is not simply a function of its occurrence frequency or formation strength.

2. It is specified that the study includes 46 NPF days, but there is no number given for the non-NPF cases. There are many claims made about the differences in NPF and non-NPF conditions in the Supplement figures, and I think that some context needs to be given as to how much more data is being considered in the non-NPF subset compared to the NPF events. For example, if the rest of the full year is included in the non-NPF subset, that could be a large quantitative difference compared to 46 days.

Response: We thank the reviewer for pointing out this missing piece of information. We agree that the number of non-NPF days should be clearly stated to provide proper context for the comparisons shown in Section 2.4.

Line 257-258: During the one-year observation, a total of 46 NPF events and 319 non-NPF days were identified.

3. Additional detail would strengthen the measurement and instrumentation section, especially for the OC/EC analyzer, WPS-1000, AE-33, and chromatograph. For

example, not all instruments are given a time resolution, and it is not clear how different observations are combined. Are certain datasets averaged over some time period? How do you combine high resolution in situ aerosol observations with 1-hr meteorological data? What are the uncertainties of each of these observations, and how do these uncertainties impact the analysis/results?

Response: We thank the reviewer for this constructive comment. We have substantially revised the measurement and instrumentation section to provide the missing details. Below, we address each specific point.

Time resolution of each instrument. We have now explicitly stated the native time resolution for each instrument in a new table (Table S1 in the Supplement) and in the revised main text. Specifically, the WPS-1000 provides particle number size distributions every 6 min; the AE-33 Aethalometer measures black carbon at 1 h, but we used 1-hour averaged data; the OC/EC analyzer (Sunset Model-4) produces hourly OC and EC concentrations; and the MARGA (online chromatograph for gases and water-soluble ions) also outputs hourly data. The meteorological data and routine air quality data are both available at 1-hour resolution. All these time resolutions are now clearly indicated in the revised manuscript

Table S1. Summary of measurement instruments, parameters, time resolution, averaging time used for analysis, and measurement uncertainties.

Station	Instrument	Parameter(s)	Time resolution	Uncertainty
The Fujian Provincial Environmental Monitoring Center Station	WPS-1000	Aerosol size distribution (10–350 nm)	6 min	±10%
	AE-33	BC	1 h	±10% (Drinovec et al., 2015)
	OC/EC Analyzer	OC, EC	1 h	OC: ±3.6%; EC: ±6.8% (Zhang et al., 2021)
	MARGA (ADI 2080)	SO_4^{2-}, NO_3^-, NH_4^+, Na^+, K^+, Ca^{2+}, Cl^-; NH_3, HNO_2, HNO_3, HCl, SO_2	1h	±5–20% (Battelle, 2009)

The Fuzhou Meteorological Bureau Station	Meteorological station	T, RH, WS, WD, precipitation	1 h	T: ±0.2°C; RH: ±4–8%; WS: ±(0.5+0.03v) m/s; WD: ±5°; precip.: ±0.4 mm/±4%
	CCNC-100	CCN number concentration and spectrum distribution	10 min per SS	±10%

Reference:

Battelle: Environmental Technology Verification Report: Applikon MARGA Semi-Continuous Ambient Air Monitoring System, U.S. Environmental Protection Agency, available at: https://nepis.epa.gov/Exe/ZyPURL.cgi?Dockey=P100FZOD.pdf (last access: 24 April 2026), 2009.

Drinovec, L., Močnik, G., Zotter, P., Prévôt, A. S. H., Ruckstuhl, C., Coz, E., Rupakheti, M., Sciare, J., Müller, T., Wiedensohler, A., and Hansen, A. D. A.: The "dual-spot" aethalometer: an improved measurement of aerosol black carbon with real-time loading compensation, Atmos. Meas. Tech., 8, 1965–1979, https://doi.org/10.5194/amt-8-1965-2015, 2015.

Zhang, X., Trzepla, K., White, W., Raffuse, S., and Hyslop, N. P.: Intercomparison of thermal–optical carbon measurements by Sunset and Desert Research Institute (DRI) analyzers using the IMPROVE_A protocol, Atmos. Meas. Tech., 14, 3217–3231, https://doi.org/10.5194/amt-14-3217-2021, 2021.

4. Additional details would also strengthen the analysis methods section:

1) The section reads a bit like a list of equations and needs more description of how these tie together and what they will be used for in later analyses.

Response: We thank the reviewer for this constructive comment. We have made the following revisions to Section 2.2

The growth rate (GR) of new particles was calculated following (Kulmala et al., 2012):

$$GR = \frac{\Delta D_m}{\Delta t} \quad (1)$$

where D_m is the median diameter of the nucleation mode particles, obtained by fitting a log-normal distribution to the particle number size distribution. Statistics of the fitting results (see Supplementary Material) demonstrate that the log-normal distribution represents the observed particle size distributions well, with the majority of fits yielding high coefficients of determination (R^2>0.85); only fits with R^2>0.7 were used to avoid propagating poor-fitting uncertainties. GR describes how rapidly particles grow from the nucleation size to larger sizes. It is later used to estimate the formation rate of new particles (Eq. 2) and condensable vapor concentration (Eq. 4) and to evaluate the competition between condensation and coagulation during NPF events.

The condensation sink (CS) reflects the rate at which condensable vapor molecules condense onto the surface of pre-existing atmospheric particles and was calculated as follows (Kulmala et al., 2012):

$$CS = 4\pi D \sum_i \beta_{M,i} \cdot D_i \cdot N_i \quad (2)$$

where D is the diffusion coefficient of the vapor (typically assumed to be sulfuric acid), N_i is the number concentration of particles in a given size bin, and β_M is a correction factor.

The coagulation sink (CoagS) reflects the ability and rate of pre-existing atmospheric particles to remove newly formed nucleation particles via coagulation. For particles of size i, the coagulation sink can be expressed as:

$$CoagS_i = \sum_j K_{ij} N_j \quad (3)$$

where N_j is the number concentration of particles in size bin j, and K_{ij} is the Brownian coagulation coefficient between particles of size j and i.

The formation rate (FR) of new particles was calculated following Kulmala et al. (2012):

$$FR = \frac{dN_{nuc}}{dt} + CoagS_{nuc} \cdot N_{nuc} + \frac{GR}{\Delta dp} + S_{losses} \quad (4)$$

where N_{nuc} is the number concentration of nucleation-mode particles. Following the definition by Kulmala et al. (2012), the nucleation-mode size range in this study was also limited to below 25 nm. $CoagS_{nuc} \cdot N_{nuc}$ is the flux of particles lost due to coagulation with pre-existing particles, where $CoagS_{nuc}$ is the coagulation sink for

nucleation-mode particles. GR/Δdp represents the flux of particles growing out of the nucleation size range (exceeding 25 nm), which is generally negligible under typical atmospheric conditions (Dal Maso et al., 2005). FR is later used to compare NPF event intensity under different meteorological and chemical conditions, and to identify periods with active nucleation. The additional loss term S_{losses} (e.g., dilution due to boundary layer growth, wall losses) was negligible under our field conditions (Dal Maso et al., 2005). For regional NPF events, transport losses can also be ignored. FR is a direct measure of NPF intensity and is later compared across different meteorological and chemical conditions.

Condensable vapor concentration (C) and source rate (Q). Assuming that particle growth is dominated by condensation of a low-volatility vapor (typically sulfuric acid), the vapor concentration can be estimated from the observed growth rate (Dal Maso et al., 2005; Kulmala et al., 2012):

$$C = A \times \frac{dDp}{dt} \quad (5)$$

where D_p is the particle diameter, and A is a constant, which has the value 1.37×10^{-7} $h\cdot cm^{-3}\cdot nm^{-1}$ for a vapor with molecular properties of sulfuric acid (Dal Maso et al., 2005). This provides an upper-limit estimate of the condensable vapor concentration, as it assumes growth is solely due to condensation of the vapor and neglects contributions from coagulation.

The CS (Eq. 2) quantifies the rate at which this vapor is removed by pre-existing particles. Under steady-state conditions (dC/dt=0), the vapor source rate Q can be derived as (Dal Maso et al., 2005):

$$Q = CS \times C \quad (6)$$

This source rate represents the net production of condensable vapor needed to maintain the observed growth and is later compared with precursor gas concentrations (e.g., SO_2) to infer the chemical pathways driving NPF.

Hygroscopicity parameter (κ_{inorg}) for inorganic species. Due to the lack of organic composition measurements, we estimated the hygroscopicity of the inorganic fraction only. The measured water-soluble ions (SO_4^{2-}, NO_3^-, NH_4^+, Cl^-) were converted to mass

concentrations of inorganic salts using the ion-pairing scheme described in Gysel et al. (2007) and Kuang et al. (2020). The following salts and their κ values (Kuang et al., 2020) were considered: $(NH_4)_2SO_4$ (κ = 0.48), NH_4NO_3 (κ = 0.58), NH_4HSO_4 (κ = 0.56), and NH_4Cl (κ = 0.93). The volume fraction of each salt was calculated using its density (also from Kuang et al., 2020). The overall inorganic hygroscopicity parameter κ_{inorg} was then obtained by volume-weighted mixing (Petters and Kreidenweis, 2007):

$$\kappa_{inorg} = \sum_i \varepsilon_i \kappa_i \quad (7)$$

where κ_i and ε_i represent the hygroscopicity parameter and volume fraction of component i in the mixture, respectively, and i denotes the number of components. This K_{inorg} represents the hygroscopicity of the inorganic aerosol components and is used as an upper-limit estimate for the total particle hygroscopicity, as organic matter (typically less hygroscopic) was not included.

The concentrations of secondary organic carbon (SOC) and primary organic carbon (POC) were estimated following (Wu and Yu, 2016):

$$POC = (OC/EC)_{min} \times EC \quad (8)$$

$$SOC = OC_{total} - (OC/EC)_{pri} \times EC \quad (9)$$

where OC_{total} is the measured OC, $(OC/EC)_{min}$ is the minimum (OC/EC) ratio during the observation period, POC is primary organic carbon, and SOC is secondary organic carbon.

The enhancement effect on cloud condensation nuclei number concentration (E_N_{CCN}) was defined as the ratio of CCN number concentration after the NPF event to that before the event (Ren et al., 2021):

$$E\_N_{CCN} = N_{CCN,\,after} / N_{CCN,\,prior} \quad (10)$$

where $N_{CCN,\,after}$, is the average CCN number concentration during the NPF event (from its start to end), and $N_{CCN,\,prior}$, is the average CCN concentration during the 2 h before the event. This factor directly links NPF to potential cloud formation: a value >1 indicates that NPF increases CCN availability.

XGBoost-SHAP framework. To quantitatively evaluate the nonlinear effects of

meteorological factors (temperature, RH) and precursor gases (NH_3, SO_2) on the particle formation rate (FR), we applied an interpretable machine learning framework combining XGBoost (Extreme Gradient Boosting) with SHAP (SHapley Additive exPlanations). A detailed description of the feature selection, model training, validation, and SHAP interpretation is provided in the supplementary material (Text S1). The main quantitative thresholds and interaction strengths derived from this analysis are discussed in Section 3.4.

2) How well does the log-normal distribution fit the observed particle size distributions (Lines 130-131)? How well does the Kulmala et al. (2012) nucleation size mode range apply to observations here (Line 135)? Under what conditions are the last two terms in the FR equation negligible (Line 137)? Does the "overall chemical composition of particles" come from observations (Line 156-157)?

Response: Thanks for your constructive comments. We also recognized a gap in the description of the log-normal distribution fit. We have now added the following content to the supplementary materials:

To ensure high data fidelity for subsequent calculations of growth rate (GR), formation rate (FR), and condensable vapor concentration, a rigorous quality control (QC) protocol was implemented. Only fits satisfying both of the following criteria were retained: (1) $R^2>0.7$, and (2) $N\leq106$ cm^{-3}. The latter criterion serves as a physically constrained upper limit to exclude spurious mathematical solutions arising from instrumental noise or extreme outliers.

As shown in Fig.S1a, the retained fits account for approximately 58% of the total dataset, a robust proportion considering the intermittent nature of new particle formation (NPF) events and the frequent occurrence of low-signal background conditions. The majority of R^2 values lie between 0.85 and 0.95, with a peak near 0.91, indicating that the log-normal model effectively captures the variance of the observed nucleation-mode particles.

Fig. S1b displays the parameter space of the fitted nucleation mode (Dpg vs. N). A high-

density cluster appears at Dpg<10 nm with elevated N, which serves as a definitive signature of NPF events. The observed downward-bending density band reflects the classical aerosol dynamic evolution: a burst of nucleated particles followed by simultaneous diameter growth (increasing Dpg) and sink-driven concentration decay (decreasing N).

The frequency distribution of σ is presented in Fig.S1c. The median σ is approximately 1.7, and most values fall within 1.5–2.0. This is highly consistent with the theoretical expectations for a well-defined, unimodal nucleation mode in atmospheric aerosol physics.

In summary, the log normal distribution provides a statistically robust (high R2), physically meaningful (reasonable D_{pg}-N evolution, σ within 1.5–2.0), and stable representation of the nucleation mode PSDs in our dataset. Fits with R2≤0.7 (e.g., during non-NPF or mixed mode conditions) are excluded from analyses requiring a well-defined nucleation mode.

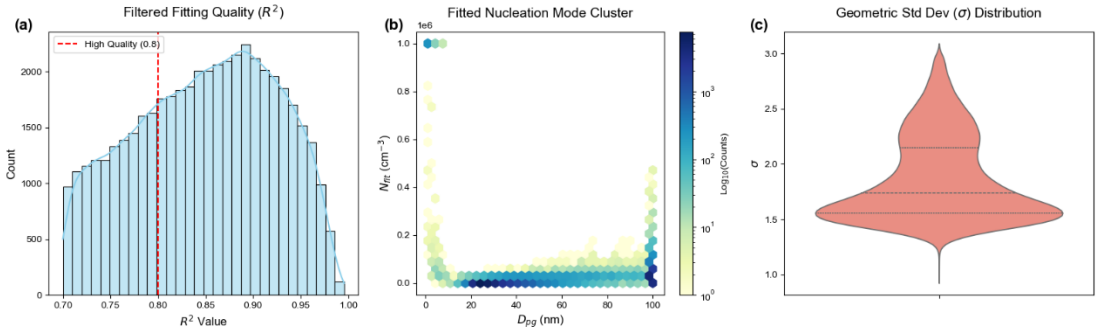

Fig. S1 Evaluation of the single-mode log-normal fitting for nucleation-mode particle size distributions (PSDs). (a) Frequency distribution of the coefficient of determination (R^2) for the retained fits (R^2>0.7). The red dashed line indicates the high-quality threshold of 0.8. (b) Density plot (hexagonal binning) of the fitted nucleation-mode parameter space showing the relationship between geometric mean diameter (D_{pg}) and total number concentration (N). The color scale represents the number of occurrences on a logarithmic scale. (c) Frequency distribution (violin plot) of the retrieved geometric standard deviation (σ). The dashed and dotted lines within the violin plot indicate the median and quartiles, respectively.

Additionally, the overall chemical composition of particles used in this study (including water-soluble ions, OC, EC, etc.) was directly measured by the instruments summarized in Table S1. Specifically, water-soluble inorganic ions (SO_4^{2-}, NO_3^-, NH_4^+, Cl^-, etc.) were measured by the MARGA (online chromatograph), and organic carbon (OC) and elemental carbon (EC) were measured by the Sunset OC/EC analyzer. These observations formed the basis for calculating the hygroscopicity parameter (κ_{inorg}) and estimating secondary organic carbon (SOC).

Table S2. Summary of measurement instruments, parameters, time resolution, averaging time used for analysis, and measurement uncertainties.

Station	Instrument	Parameter(s)	Time resolution	Uncertainty
The Fujian Provincial Environmental Monitoring Center Station	WPS-1000	Aerosol size distribution (10–350 nm)	6 min	±10%
	AE-33	BC	1 h	±10% (Drinovec et al., 2015)
	OC/EC Analyzer	OC, EC	1 h	OC: ±3.6%; EC: ±6.8% (Zhang et al., 2021)
	MARGA (ADI 2080)	SO_4^{2-}, NO_3^-, NH_4^+, Na^+, K^+, Ca^{2+}, Cl^-; NH_3, HNO_2, HNO_3, HCl, SO_2	1h	±5–20% (Battelle, 2009)
The Fuzhou Meteorological Bureau Station	Meteorological station	T, RH, WS, WD, precipitation	1 h	T: ±0.2°C; RH: ±4–8%; WS: ±(0.5+0.03v) m/s; WD: ±5°; precip.: ±0.4 mm/±4%
	CCNC-100	CCN number concentration and spectrum distribution	10 min per SS	±10%

Minor Comments

1. Lines 51-60: What factors govern formation rate and growth rate?

Response: Thank you very much for raising this important point. We will add a clearer explanation in the revised manuscript.

Line 62-67: The availability of precursor vapors and the atmospheric chemical

environment play decisive roles. H_2SO_4 is a key nucleating species, and its stabilizing co-components, such as ammonia (NH_3) and amines, can dramatically enhance FR (Dunne et al., 2016; Yao et al., 2018; Kirkby et al., 2016). For particle growth, condensation of low-volatility compounds is the dominant process. Sipilä et al. (2010) showed experimentally that early-stage growth is primarily driven by H2SO4 condensation.

2. Lines 55-56: How is NPF occurrence constrained by temperature and humidity?

Response: Thank you very much for raising this important point. We will add a clearer explanation in the revised manuscript.

Line 69-78: Low temperatures promote nucleation, whereas high temperatures suppress it (Sipilä et al., 2010; Dunne et al., 2016; Yu et al., 2017). Dunne et al. (2016) further showed that at low temperatures, the ion-enhancement effect is weak due to suppressed evaporation of neutral clusters, while at ambient temperatures, ions can increase the nucleation rate by about a factor of 15. Consequently, neglecting temperature dependence leads to a marked overestimation of NPF and CCN concentrations in summer (Yu et al., 2017). Hamed et al. (2011), based on observations at multiple continental sites, found that NPF events predominantly occur at relative humidity below 60% and are rare above 80%. The reason is that high relative humidity reduces ultraviolet radiation, lowering the production of OH and H_2SO_4; meanwhile, hygroscopic growth enhances the condensation sink, thereby suppressing new particle formation.

Reference:

Dunne, E. M., Gordon, H., Kürten, A., Almeida, J., Duplissy, J., Williamson, C., Ortega, I. K., Pringle, K. J., Adamov, A., Baltensperger, U., Barmet, P., Benduhn, F., Bianchi, F., Breitenlechner, M., Clarke, A., Curtius, J., Dommen, J., Donahue, N. M., Ehrhart, S., Flagan, R. C., Franchin, A., Guida, R., Hakala, J., Hansel, A., Heinritzi, M., Jokinen, T., Kangasluoma, J., Kirkby, J., Kulmala, M., Kupc, A., Lawler, M. J., Lehtipalo, K., Makhmutov, V., Mann, G., Mathot, S., Merikanto, J., Miettinen, P., Nenes, A., Onnela, A., Rap, A., Reddington, C. L. S., Riccobono, F., Richards, N. A. D., Rissanen, M. P., Rondo, L., Sarnela, N., Schobesberger, S., Sengupta, K., Simon, M., Sipilä, M., Smith, J. N., Stozkhov, Y., Tomé, A., Tröstl, J., Wagner, P. E., Wimmer, D., Winkler, P. M., Worsnop, D. R., and Carslaw, K. S.: Global atmospheric particle formation from CERN CLOUD measurements, Science, 354, 1119–1124,

https://doi.org/10.1126/science.aaf2649, 2016.

Maso, M. D., Kulmala, M., Riipinen, I., Wagner, R., Hussein, T., Aalto, P., and Lehtinen, K.: Formation and growth of fresh atmospheric aerosols: eight years of aerosol size distribution data from SMEAR II, hyytiälä, finland, Boreal Environ. Res., 2005.

Sipilä, M., Berndt, T., Petäjä, T., Brus, D., Vanhanen, J., Stratmann, F., Patokoski, J., Mauldin, R. L., Hyvärinen, A.-P., Lihavainen, H., and Kulmala, M.: The role of sulfuric acid in atmospheric nucleation, Science, 327, 1243–1246, https://doi.org/10.1126/science.1180315, 2010.

Yu, F., Luo, G., Nadykto, A. B., and Herb, J.: Impact of temperature dependence on the possible contribution of organics to new particle formation in the atmosphere, Atmos. Chem. Phys., 17, 4997–5005, https://doi.org/10.5194/acp-17-4997-2017, 2017.

3. Line 63: Can you be more specific on what the "various atmospheric conditions" refer to?

   Response: Thank you for pointing this out. By "various atmospheric conditions," we meant different environments such as urban, suburban, rural, mountain, and varying levels of pollution. We have clarified this in the revised manuscript.

   Line 87-88: Observations across different sites (e.g., mountain, urban) have shown that NPF events typically lead to a significant increase in N_{CCN} (Kuwata et al., 2008; Yue et al., 2011; Fan et al., 2018).

4. Line 76/77: What exact mechanisms are being referred to here? Different ones than nucleation mechanisms listed in Line 72?

   Response: Thank you for pointing this out. We have made the following revisions:

   Line 101-103: Currently, understanding how regional variations in atmospheric oxidants and precursors affect the growth of newly formed particles to CCN sizes, especially the quantification of their CCN efficiency, remains a challenge and a frontier in current research

5. Line 86-90: It seems like these first two sentences could be combined to be more concise.

   Response: Thank you for your helpful suggestion. We have combined the two sentences in lines 86–90 to improve conciseness.

Line 114-117: Observation data for this study were collected from June 1, 2021, to May 30, 2022, during comprehensive atmospheric environmental observations conducted at the Fujian Provincial Environmental Monitoring Center Station (26.11°N, 119.30°E, altitude 65 m) and the Fuzhou Meteorological Bureau Station (26.05°N, 119.26°E, altitude 18 m).

6. Line 103: OPC is not defined. OPC.

Response: Thank you for your helpful suggestion. We have given the complete name.

Line 131-133: To maintain counting accuracy, the instrument was regularly calibrated for T gradient, flow rate, pressure, SS, and the optical particle counter (OPC) using standard ammonium sulfate according to the method by Rose et al. (2008).

7. Line 140: This seems to be a repeat equation in the text.

Response: Thank you for your careful reading of our manuscript. We have correct that the equation presented in line 140 is a repetition.

Line 177-181:

The condensation sink (CS) reflects the rate at which condensable vapor molecules condense onto the surface of pre-existing atmospheric particles and was calculated as follows (Kulmala et al., 2012):

$$CS = 4\pi D \sum_i \beta_{M,i} \cdot D_i \cdot N_i \quad (2)$$

where D is the diffusion coefficient of the vapor (typically assumed to be sulfuric acid), N_i is the number concentration of particles in a given size bin, and β_M is a correction factor.

8. Line 201: Can you clarify that pollution levels were higher on NPF days in spring and winter? From Fig. S3 at first glance it looks like pollution levels are highest in spring and summer.

Response: Thank you very much for raising this important point. We will add a clearer explanation in the revised manuscript.

Line 274-276: It should be noted that the absolute $PM_{2.5}$ and PM_{10} in winter and spring were still relatively high compared to other seasons (Fig. S3), implying that even on

NPF days.

Line 280-285: Although winter had heavy background pollution, Fig.S4 shows that the gaseous precursor SO_2 concentration on NPF days was significantly higher than on non-NPF days (winter: 0.88 vs. 0.76 $\mu g \cdot m^{-3}$; spring: 0.64 vs. 0.53 $\mu g \cdot m^{-3}$). This indicates that in polluted seasons, high gaseous precursors can overcome the inhibitory effect of a high CS and thus trigger nucleation. In contrast, NPF days in summer and Fall exhibited a distinctly clean background, with NH_3 and HNO_2 significantly lower than on non-NPF days (Fig.S4).

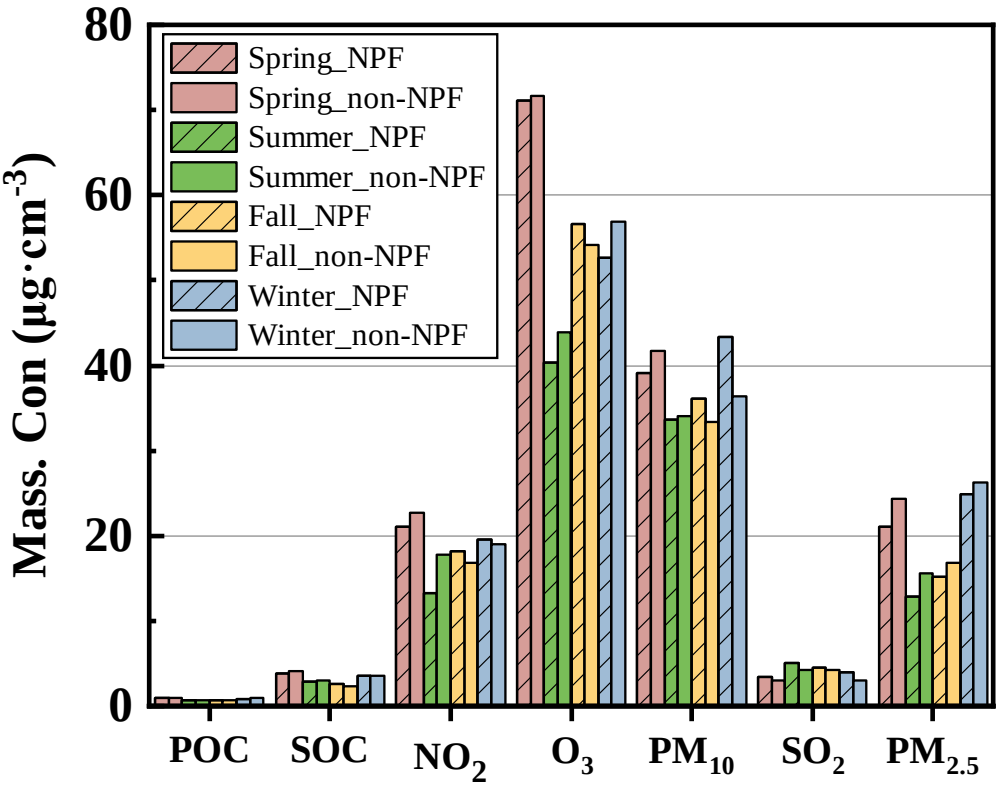

Fig.S3 Mass concentrations of particulate pollutants between NPF days and non-NPF days.

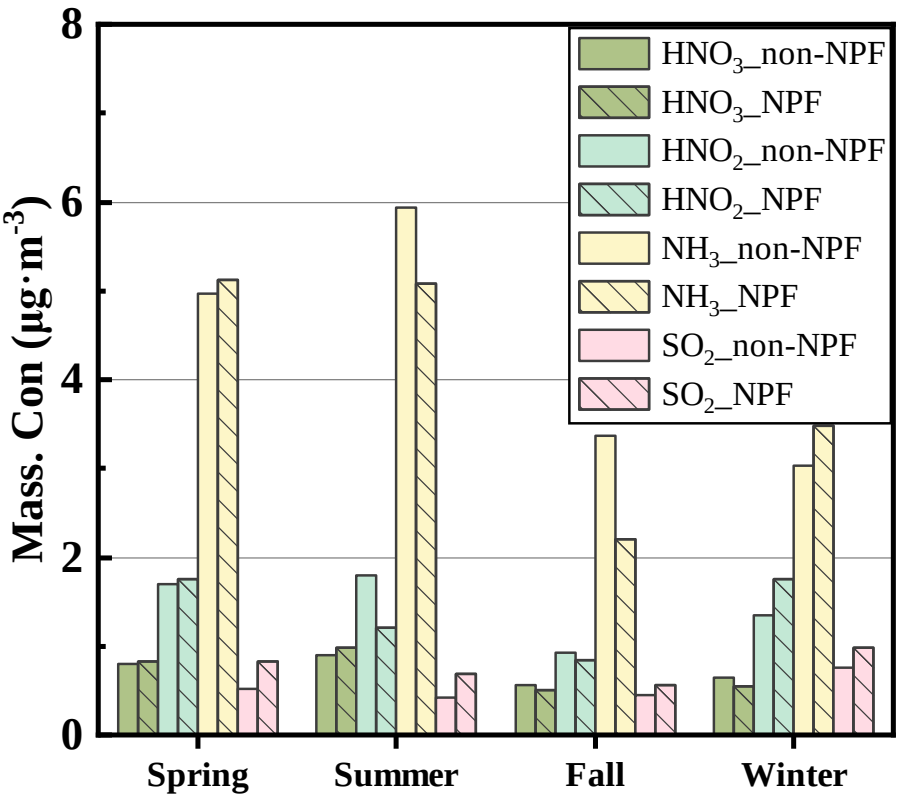

Fig.S4 Mass concentrations of precursor gases (e.g., SO_2, NO_2, O_3, NH_3) between NPF days and non-NPF days.

9. Line 205-206: I am not seeing that secondary organic ion concentrations are similar between NPF and non-NPF days in spring from Fig. S4. Is this a typo?

   Response: Thank you very much for raising this important point. We will add a clearer explanation in the revised manuscript.

   Line 288-292: However, spring presents a special case in that the SNA (sulfate, nitrate, and ammonium) concentrations on NPF days were comparable to those on non-NPF days (SO_4^{2-}: 4.35 vs. 4.27 μg·m^{-3}). This indicates that spring NPF events are driven by high precursor concentrations. Even when the background particle level is high, the abundant supply of gaseous precursors (Fig. S4) can still overcome the inhibition and trigger NPF events.

10. Line 208-209: Is the hygroscopicity parameter calculated for only nucleation mode particles? Or for all observed aerosols?

    Response: Thank you for raising this important point. In the original manuscript, the hygroscopicity parameter (κ_{inorg}) was calculated for all measured water-soluble

inorganic ions in $PM_{2.5}$, not specifically for nucleation mode particles alone. This represents the bulk aerosol hygroscopicity of the submicron fraction, which includes particles of all sizes (from nucleation to accumulation mode). We agree that the original wording was ambiguous. To clarify, we have added the following sentence in the revised manuscript (Section 2.3, Eq. 7):

Lin 216-228:

Hygroscopicity parameter (κ_{inorg}) for inorganic species. Due to the lack of organic composition measurements, we estimated the hygroscopicity of the inorganic fraction only. The measured water-soluble ions (SO_4^{2-}, NO_3^-, NH_4^+, Cl^-) were converted to mass concentrations of inorganic salts using the ion-pairing scheme described in Gysel et al. (2007) and Kuang et al. (2020). The following salts and their κ values (Kuang et al., 2020, Table S2) were considered: $(NH_4)_2SO_4$ (κ = 0.48), NH_4NO_3 (κ = 0.58), NH_4HSO_4 (κ = 0.56), and NH_4Cl (κ = 0.93). The volume fraction of each salt was calculated using its density (also from Kuang et al., 2020). The overall inorganic hygroscopicity parameter κ_{inorg} was then obtained by volume-weighted mixing (Petters and Kreidenweis, 2007):

$$\kappa_{inorg} = \sum_i \varepsilon_i \kappa_i \quad (7)$$

where κ_i and ε_i represent the hygroscopicity parameter and volume fraction of component i in the mixture, respectively, and i denotes the number of components. This κ_{inorg} represents the hygroscopicity of the inorganic aerosol components and is used as an upper-limit estimate for the total particle hygroscopicity, as organic matter (typically less hygroscopic) was not included.

11. Line 266-267 & Fig. S8: It looks like kappa decreases with time in fall and that there's a small net decrease in spring. Summer appears to be the only season with a substantial increase, but it also oscillates quite a bit. This is explained more in the next paragraph, but it is not immediately clear from Fig. S8 that kappa generally increases following NPF events in the other 3 seasons.

Response: Thank you for your careful observation regarding Figure S8 and the

corresponding explanation in the text.

In response to your comment, and also following a valuable suggestion from another reviewer, we have refined our calculation of κ_{inorg} by including chloride (Cl^-) as an additional inorganic component. The revised κ values and their seasonal variations have been re-analyzed, and the updated figure (originally Fig. S8, now renumbered as Fig. S10) now more clearly demonstrates that κ_{inorg} generally increases after NPF events in all four seasons, although the magnitude of increase varies.

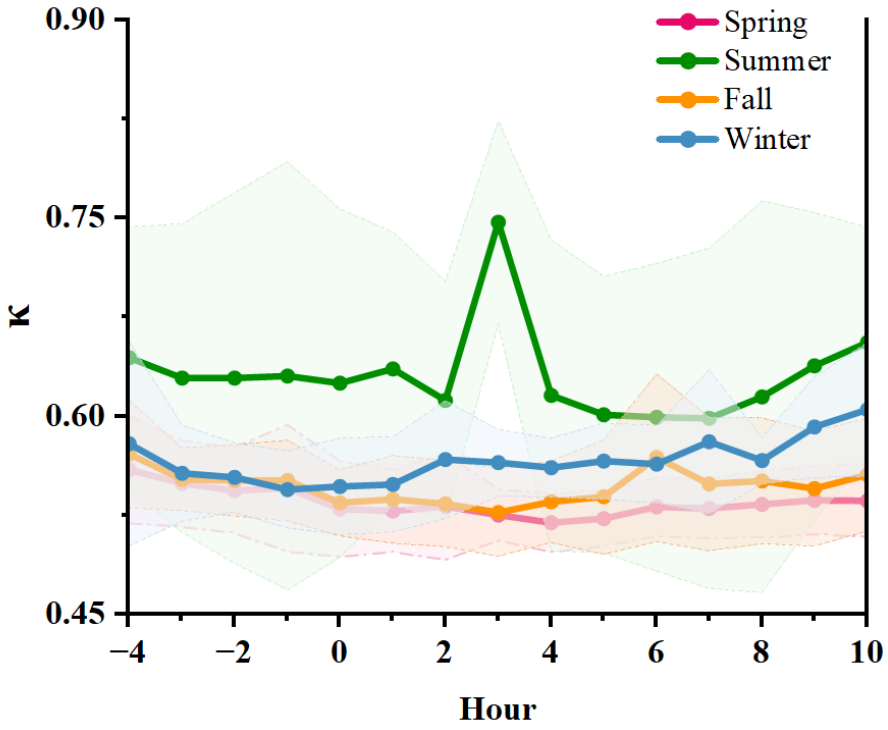

Fig.S10 Temporal evolution of the particle hygroscopicity parameter (κ_{inorg}) during NPF events. The x-axis follows the same normalized time scale as defined in Fig. 4 (t=0 h represents NPF event start). Shaded bands indicate ±1σ standard deviation.

12. Fig. S9: Would it be possible to put all panels on the same x-axis scale to make it easier to compare differences in magnitude between seasons?

Response: Thank you for this suggestion. We have revised Fig. S9 so that all panels now share the same x-axis scale. This change indeed facilitates a clearer comparison of seasonal differences. The updated figure has been included in the revised manuscript.

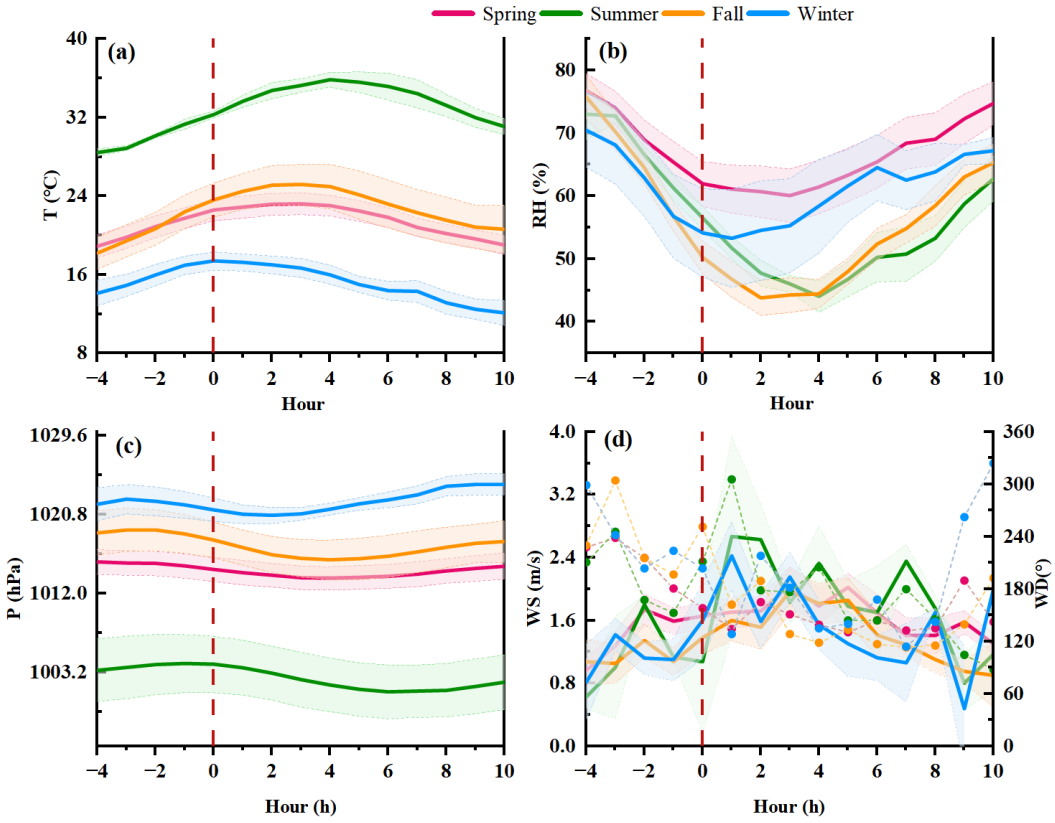

Fig. S11 Temporal evolution of meteorological parameters, including (a) temperature (T), (b) relative humidity (RH), (c) pressure (P), and (d) wind speed (WS, solid lines) and wind direction (WD, dashed lines with dots) during NPF events across four seasons. The x-axis follows the same normalized time scale as defined in Fig. 4, where t = 0 h represents the onset of the NPF event. In panels (a)-(c), solid lines represent the median values, and shaded bands indicate. In panel (d), the left y-axis corresponds to WS, while the right y-axis corresponds to WD.

13. Line 275: This section discusses meteorology in addition to chemistry. Would it make sense to add meteorology into the section title?

Response: We thank the reviewer for the careful reading and the thoughtful suggestion. The section in question (Section 3.3, originally titled "Influence of chemical composition on NPF events") indeed briefly describes meteorological conditions such as temperature, wind direction, and relative humidity as part of the seasonal context. However, the primary focus of this section is to elucidate how the chemical composition of aerosols and precursor gases (e.g., NH_3, SO_2, sulfate, nitrate, BC, POC, SOC) drives

the observed seasonal variations in NPF parameters (FR, GR, CS, etc.). Meteorological variables are mentioned only as background environmental settings that do not constitute the core analytical theme. Adding "meteorology" to the section title would risk overemphasizing their role and potentially misleading readers about the main message of this section. Therefore, we prefer to keep the original title unchanged. We have, nonetheless, clarified in the revised text that meteorological conditions serve as contextual background, while the mechanistic interpretation remains focused on chemical drivers. We hope the reviewer finds this explanation reasonable.

14. Line 350-351: If this section is about spring, I think the reference needs to be changed to Fig. S12a. Also, at SS = 0.4%, I do not see what would be considered a "rapid decline" in CCN from that panel.

Response: Thank you very much for raising this important point. First, regarding the figure citation error, we have corrected it in the revised manuscript. Second, concerning the description of a "rapid decline" at SS = 0.4%: after re-examining the data, we found that the decrease in N_{CCN} at this supersaturation level is indeed modest (approximately 7%), so the wording "rapid decline" was inappropriate. However, at high SS (e.g., 0.8% and 1.0%), the decline is substantially more pronounced (exceeding 25%). To avoid misleading readers, we have revised the text as follows:

Line 483-485: N_{CCN} (0.4 % SS, the same as below) increased from a pre-event average (-4 to -1 h) of about 2636 cm^{-3} to 3192 cm^{-3} at 4 h, then decreased slowly from 4 to 6 h, with a larger decline at higher supersaturations (Fig. S17a).

RC2:

This manuscript presents a one-year observational study of new particle formation (NPF) events and their impact on cloud condensation nuclei (CCN) in a Chinese coastal city. A total of 46 NPF events were identified, representing an overall frequency of 12.7%. The study provides a detailed seasonal analysis of NPF characteristics, including particle formation rates (FR), growth rates (GR), and their interactions with atmospheric chemistry and aerosol composition. The results reveal pronounced seasonal contrasts. For example, spring shows the highest FR and NPF frequency but exhibits suppressed particle growth and negligible CCN enhancement; in contrast, summer demonstrates the highest GR and the most significant CCN enhancement effect. While the findings are interesting, the manuscript consists largely of measurement results, which may be more suitable for publication as a measurement report unless the authors can substantially expand on the novelty of the study beyond data reporting. Specific comments are provided below:

Response: We appreciate the time and effort that the editor and the reviewers dedicated to providing feedback on our manuscript. We are grateful for the insightful comments and valuable improvements to our paper. We have incorporated most of the suggestions made by the reviewers. According to your suggestion, we modified the manuscript in detail and marked the revised contents with red font.

1. Observation sites: The methods describe measurements from two distinct sites: the Fujian Provincial Environmental Monitoring Center Station (central urban) and the Fuzhou Meteorological Bureau Station (near the river, southern urban). However, the results and discussion present integrated or representative data without clarifying how data from these two locations were merged, compared, or selected for the analyses in Figures 3–7. These locations are potentially subject to different local influences (e.g., intense human activity vs. marine/river impacts). The authors have missed an opportunity to use the dual-site setup to examine local influences. Were any differences observed? Please clarify.

Response: We thank the reviewer for this constructive comment.

1) The two original observation sites are only about 8 km apart (urban: 26.11°N, 119.30°E; riverside: 26.05°N, 119.26°E), so their local environments are not expected to be drastically different. Because the two sites measured completely different variables (aerosol chemistry at the urban station vs. CCN and meteorology at the riverside station), no overlapping measurements exist for direct comparison. Therefore, we selected the national monitoring station near the meteorological bureau (1282A, representing the riverside area) and compared it with the station at the Environmental Monitoring Center (1283A, representing the urban area). Using data from 46 NPF event days (as identified at the urban station), we compared six pollutants ($PM_{2.5}$, NO_2, O_3, PM_{10}, SO_2, and CO). The results are presented in Table S2. The two sites show generally comparable pollutant levels, reflecting a well-mixed regional background. Nevertheless, the urban site exhibits slightly higher NO_2 (+4.7%) and CO (+4%), indicating a modest anthropogenic influence, while the riverside site has marginally higher $PM_{2.5}$ and PM_{10}, possibly due to local sources or humidity effects. These small differences confirm that the two sites are subject to distinct local influences (urban vs. riverside), as noted by the reviewer. We have added this discussion in Section 2.1 (Lines 156–160).

   Line 156-160: Given the short distance (about 8 km) and the regional background homogeneity, the local environments of the two sites are not expected to be drastically different, although each is influenced by its specific surroundings (urban vs. riverside). A comparison of air pollutant concentrations between the two sites using nearby national monitoring stations (Table S2).

Table S2. Comparison of air pollutant concentrations at the two sites during NPF event days (mean ± standard deviation, n = 46 days).

Factors	Riverside site (1282A)	Urban site (1283A)	Difference (%)
$PM_{2.5}$ (μg/m³)	19.6±9.7	17.6±8.7	–10.2
NO_2 (μg/m³)	19.3±6.8	20.2±8.5	+4.7

O_3 (μg/m³)	61.4±19.5	61.8±18.3	+0.7
PM_{10} (μg/m³)	38.3±14.0	37.6±13.8	–1.8
SO_2 (μg/m³)	3.9±1.2	3.9±1.0	0
CO (mg/m³)	0.50±0.10	0.52±0.15	+4

2) All raw measurements (aerosol size distribution, chemical composition, BC, etc.) were obtained from the instruments listed in Table S1, with their respective observation sites indicated in the table. The derived parameters (FR, GR, CS, κ_inorg, etc.) were then calculated from these raw data following the methods in Section 2.3. Specifically, all data used in Figures 3–7 (WPS-1000, MARGA, OC/EC, AE-33) come from the Urban Environmental Monitoring Center. The CCN data from the meteorological bureau station (riverside site) are used only in later sections (Figures 8–9), and meteorological data are used only for contextual interpretation. The two stations measure different variables. The comparison results in Table S2 confirm that the regional background is well mixed, supporting the representativeness of the urban-site data used in Figures 3–7.

Table S3. Summary of measurement instruments, parameters, time resolution, averaging time used for analysis, and measurement uncertainties.

Station	Instrument	Parameter(s)	Time resolution	Uncertainty
The Fujian Provincial Environmental Monitoring Center Station	WPS-1000	Aerosol size distribution (10–350 nm)	6 min	±10%
	AE-33	BC	1 h	±10% (Drinovec et al., 2015)
	OC/EC Analyzer	OC, EC	1 h	OC: ±3.6%; EC: ±6.8% (Zhang et al., 2021)
	MARGA (ADI 2080)	SO_4^{2-}, NO_3^-, NH_4^+, Na^+, K^+, Ca^{2+}, Cl^-; NH_3, HNO_2, HNO_3, HCl, SO_2	1h	±5–20% (Battelle, 2009)
The Fuzhou Meteorological Bureau Station	Meteorological station	T, RH, WS, WD, precipitation	1 h	T: ±0.2°C; RH: ±4–8%; WS: ±(0.5+0.03v) m/s; WD: ±5°; precip.: ±0.4 mm/±4%
	CCNC-100	CCN number concentration and spectrum distribution	10 min per SS	±10%

Reference:

Battelle: Environmental Technology Verification Report: Applikon MARGA Semi-Continuous Ambient Air Monitoring System, U.S. Environmental Protection Agency, available at: https://nepis.epa.gov/Exe/ZyPURL.cgi?Dockey=P100FZOD.pdf (last access: 24 April 2026), 2009.

Drinovec, L., Močnik, G., Zotter, P., Prévôt, A. S. H., Ruckstuhl, C., Coz, E., Rupakheti, M., Sciare, J., Müller, T., Wiedensohler, A., and Hansen, A. D. A.: The "dual-spot" aethalometer: an improved measurement of aerosol black carbon with real-time loading compensation, Atmos. Meas. Tech., 8, 1965–1979, https://doi.org/10.5194/amt-8-1965-2015, 2015.

Zhang, X., Trzepla, K., White, W., Raffuse, S., and Hyslop, N. P.: Intercomparison of thermal–optical carbon measurements by Sunset and Desert Research Institute (DRI) analyzers using the IMPROVE_A protocol, Atmos. Meas. Tech., 14, 3217–3231, https://doi.org/10.5194/amt-14-3217-2021, 2021.

2. Line 151: The constant A is given as 1.37×10^{-7} $h\cdot cm^{-3}\cdot nm^{-1}$. Please provide a reference for this value.

Response: We thank the reviewer for pointing out this missing reference. The constant $A=1.37\times10^{-7} h\cdot cm^{-3}\cdot nm^{-1}$ is taken from (Maso et al., 2005). In that paper, the authors derived this constant based on the molecular properties of sulfuric acid (vapor molecular weight, diffusion coefficient, and density) under the assumption that particle growth is driven solely by condensation of a low-volatility vapor. Specifically, the constant A is obtained by integrating the mass flux equation and relates the observed growth rate GR to the vapor concentration C via $C=A\times GR$. The same value has been widely used in subsequent NPF studies (Kulmala et al., 2012; Nieminen et al., 2010). We have now added the citation to Dal Maso et al. (2005) in the revised manuscript. The sentence now reads:

Line 205-206: where Dp is the particle diameter, and A is a constant, which has the value 1.37×10^{-7} $h\cdot cm^{-3}\cdot nm^{-1}$ for a vapor with molecular properties of sulfuric acid (Dal

Maso et al., 2005).

Reference:

Kulmala, M., Petäjä, T., Nieminen, T., Sipilä, M., Manninen, H. E., Lehtipalo, K., Dal Maso, M., Aalto, P. P., Junninen, H., Paasonen, P., Riipinen, I., Lehtinen, K. E. J., Laaksonen, A., and Kerminen, V.-M.: Measurement of the nucleation of atmospheric aerosol particles, Nat. Protoc., 7, 1651–1667, https://doi.org/10.1038/nprot.2012.091, 2012.

Maso, M. D., Kulmala, M., Riipinen, I., Wagner, R., Hussein, T., Aalto, P., and Lehtinen, K.: Formation and growth of fresh atmospheric aerosols: eight years of aerosol size distribution data from SMEAR II, hyytiälä, finland, Boreal Environ. Res., 2005.

Nieminen, T., Lehtinen, K. E. J., and Kulmala, M.: Sub-10 nm particle growth by vapor condensation – effects of vapor molecule size and particle thermal speed, Atmos. Chem. Phys., 10, 9773–9779, https://doi.org/10.5194/acp-10-9773-2010, 2010.

3. Lines 152–159: The calculation of the hygroscopicity parameter κ (Equation 6) assumes an internal mixture of organics, $(NH_4)_2SO_4$, and NH_4NO_3. Although this is a common simplification, the authors should briefly acknowledge this assumption and its limitations. Specifically, neglecting other inorganic ions (e.g., Cl^-, sea-salt components, which may be relevant in a coastal city) and assuming immediate mixing could affect the accuracy of the derived κ values, especially in discussions of seasonal hygroscopicity contrasts.

Additionally, while the method section provides κ values for pure $(NH_4)_2SO_4$ (0.61) and NH_4NO_3 (0.67), it does not specify the κ value assigned to the organic component. This is a required input for the calculation. Please clarify.

Response: We sincerely thank the reviewer for this insightful comment. In our original analysis, we followed a common approach that was originally developed for inland sites where chloride concentrations are typically low, and therefore, we did not include Cl^- in the hygroscopicity calculation. However, as the reviewer rightly pointed out, Fuzhou

is a coastal city where Cl- may contribute non-negligibly to aerosol composition. We acknowledge that our previous treatment was an oversimplification for this specific environment.

Following the reviewer's suggestion, we have now fully revised the calculation of the hygroscopicity parameter. Specifically, we have incorporated Cl^- into the ion-pairing scheme following Gysel et al. (2007) and Kuang et al. (2020). The measured concentrations of SO_4^{2-}, NO_3^-, NH_3^+, and Cl^- are now used to form NH_4Cl, $(NH_4)_2SO_4$, NH_4HSO_4, and NH_4NO_3 sequentially. This allows us to derive a revised inorganic hygroscopicity parameter (κ_{inorg}) that better reflects the aerosol properties in the coastal atmosphere of Fuzhou.

At the same time, we have clarified in the revised manuscript that our calculation only represents the inorganic fraction. Because we lack volume fraction data for organic species, we do not assign a κ value to organics, and we therefore explicitly state that κ_{inorg} should be considered as an upper-limit estimate of total aerosol hygroscopicity. We have also corrected the misleading wording that previously suggested an internal mixture including organics, and we now clearly discuss the limitations of the internal mixing assumption.

Line 216-228:

Hygroscopicity parameter (κ_{inorg}) for inorganic species. Due to the lack of organic composition measurements, we estimated the hygroscopicity of the inorganic fraction only. The measured water-soluble ions (SO_4^{2-}, NO_3^-, NH_4^+, Cl^-) were converted to mass concentrations of inorganic salts using the ion-pairing scheme described in Gysel et al. (2007) and Kuang et al. (2020). The following salts and their κ values (Kuang et al., 2020) were considered: $(NH_4)_2SO_4$ ($\kappa = 0.48$), NH_4NO_3 ($\kappa = 0.58$), NH_4HSO_4 ($\kappa = 0.56$), and NH_4Cl ($\kappa = 0.93$). The volume fraction of each salt was calculated using its density (also from Kuang et al., 2020). The overall inorganic hygroscopicity parameter κ_{inorg} was then obtained by volume-weighted mixing (Petters and Kreidenweis, 2007):

$$\kappa_{inorg} = \sum_i \varepsilon_i \kappa_i \quad (7)$$

where κ_i and ε_i represent the hygroscopicity parameter and volume fraction of component i in the mixture, respectively, and i denotes the number of components. This κ_{inorg} represents the hygroscopicity of the inorganic aerosol components and is used as an upper-limit estimate for the total particle hygroscopicity, as organic matter (typically less hygroscopic) was not included.

4. Figures 5–6: Please explain the color-shaded regions in the plots. What do they represent (e.g., 1σ standard deviation, confidence interval, or other)?

Response: We greatly appreciate your insightful comments on our manuscript. These suggestions have helped us improve the clarity and interpretability of our results. Below we provide the revised.

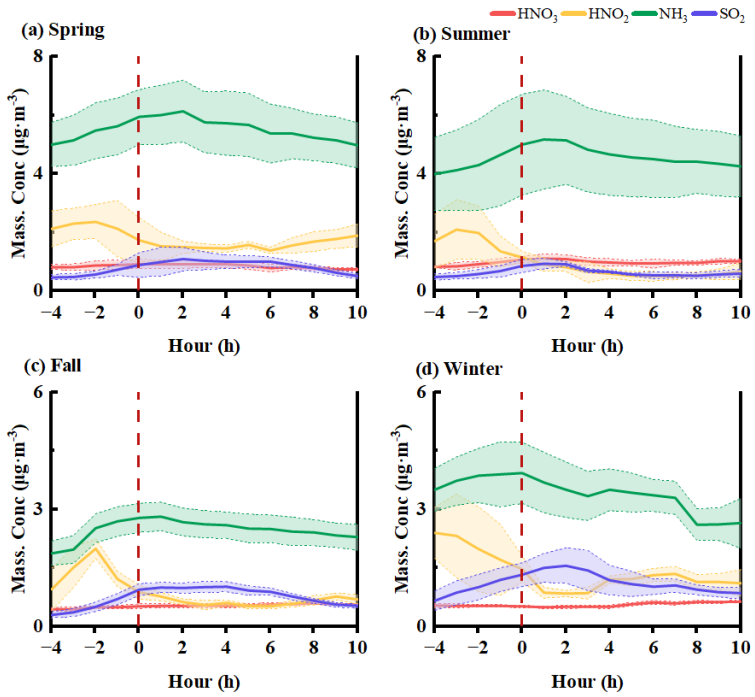

Fig. 5 The evolution of relevant trace gases (SO_2, NH_3, NO_2) before, during, and after NPF events for (a) spring, (b) summer, (c) fall, and (d) winter. The x-axis follows the same normalized time scale as defined in Fig. 4 (t=0 h represents NPF event start). Shaded bands indicate ±1σ standard deviation

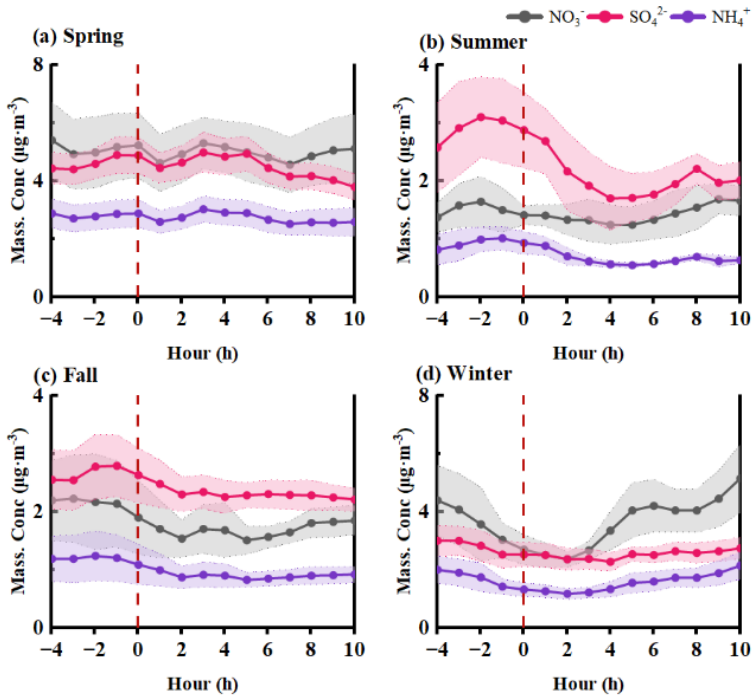

Fig. 6 The evolution of major secondary inorganic ions (SO_4^{2-}, NO_3^-, NH_4^+) before, during, and after NPF events for each season. The x-axis follows the same normalized time scale as defined in Fig. 4 (t=0 h represents NPF event start). Shaded regions represent ±1σ standard deviation across events

5. Sections 3.2 and 3.3: The results are presented by sequentially listing findings for the four seasons. Condensing this portion and adding a concluding paragraph at the end of each section that summarizes the key observations and seasonal differences would help readers better grasp the results of the study.

Response: We greatly appreciate your insightful comments on our manuscript. These suggestions have helped us improve the clarity and interpretability of our results. Below we provide the revised.

Line 358-361: In summary, spring shows the highest FR (7.13 $cm_{-3}\cdot s^{-1}$) but the lowest GR (3.69 $nm\cdot h^{-1}$) due to a large CS, indicating strong nucleation yet suppressed growth. Summer achieves the highest GR (peak 11.68 $nm\cdot h^{-1}$) and the cleanest background (lowest CS), where growth dominates over formation. Fall and winter exhibit low FR and GR with delayed growth, reflecting weaker NPF intensity.

Line 437-440: In summary, in spring, high NH_3 and photochemistry drive strong

nucleation, but high CS and secondary inorganic salts suppress growth. Summer marine air masses provide low CS and high hygroscopicity (κ_{inorg} > 0.6), favoring efficient growth, while fall and winter continental emissions (BC, POC) lower κ_{inorg} ($\leqslant$0.55) and limit NPF intensity.

6. Line 277: The phrase "Before the NPF event" is ambiguous. Does it refer to "before 9 a.m."? Please specify the time. Also, clearly define t = 0 on the x-axis of Figures 4–6.

Response: We thank the reviewer for pointing out this ambiguity. In our analysis, all NPF events were aligned by their start time (defined as the time when the nucleation-mode particle number concentration begins a sustained increase and a new mode appears in the size distribution). This start time is denoted as t = 0 h on the x-axis of Figures 4–6 and in the related text. The time window from t = –4 h to t = 0 h represents the 4 hours before the NPF event, and t = 0 h to t = 10 h represents the 10 hours after the onset of the event.

Following the reviewer's suggestion, we have added a clear explanation of this normalized time axis directly into the caption of Figure 4, as this is the most prominent figure showing time-dependent NPF parameters. The revised caption is as follows:

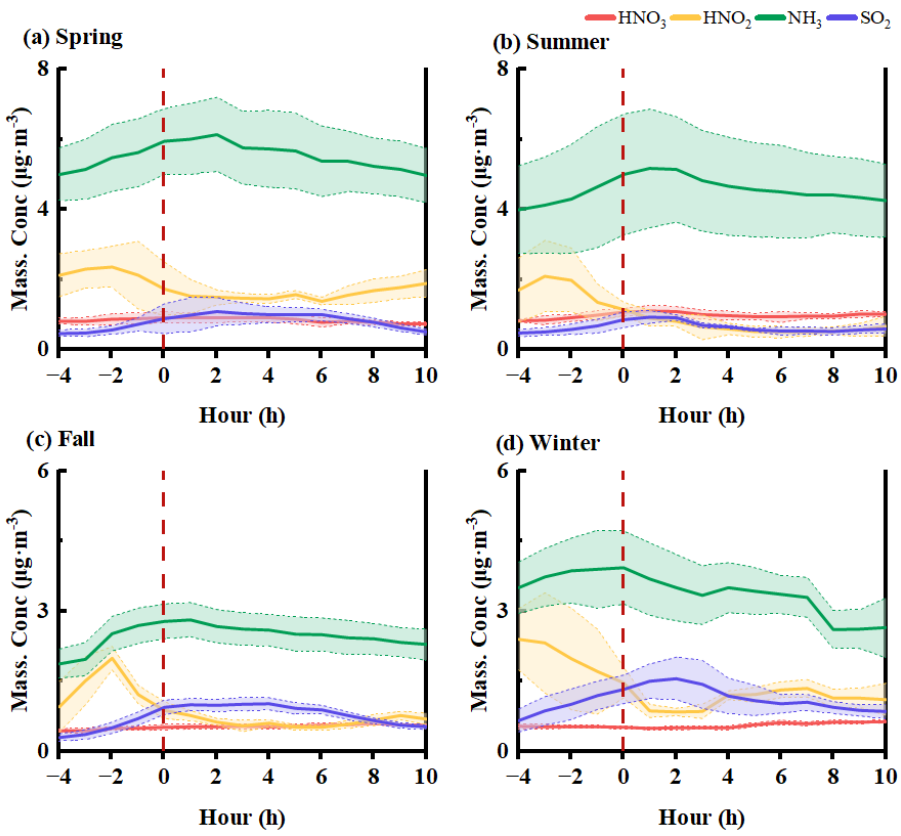

Fig. 5 The evolution of relevant trace gases (SO_2, NH_3, HNO_2, HNO_3) before, during, and after NPF events for (a) spring, (b) summer, (c) fall, and (d) winter. The x-axis follows the same normalized time scale as defined in Fig. 4 (t=0 h represents NPF event start). Shaded bands indicate ±1σ standard deviation

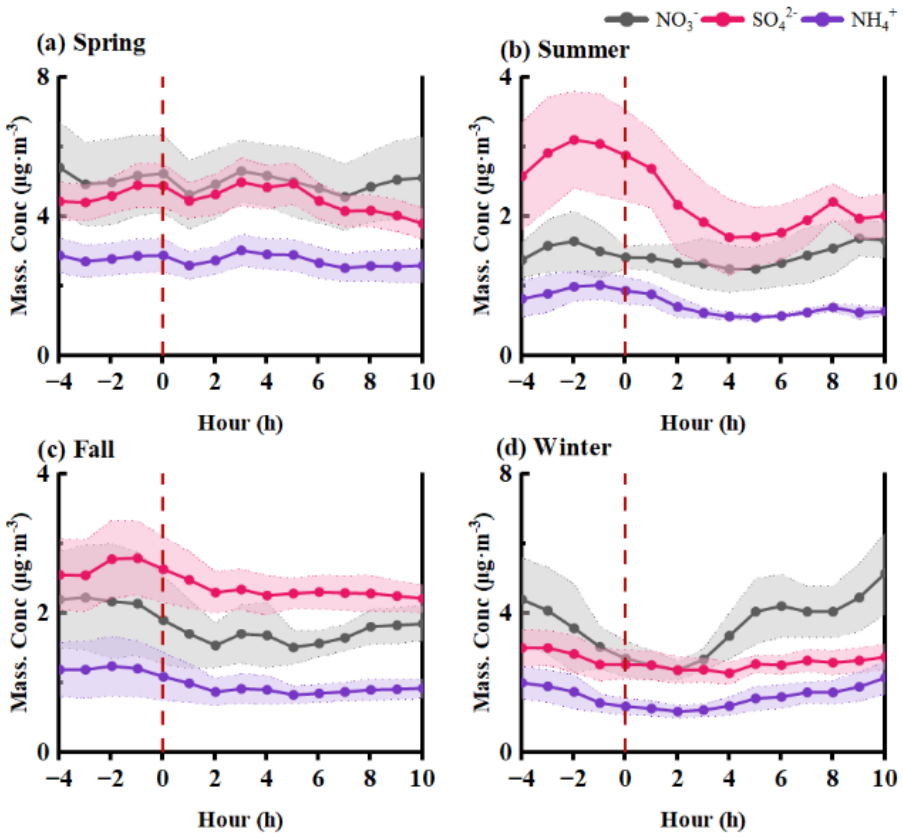

Fig. 1 The evolution of major secondary inorganic ions (SO_4^{2-}, NO_3^-, NH_4^+) before, during, and after NPF events for each season. The x-axis follows the same normalized time scale as defined in Fig. 4 (t=0 h represents NPF event start). Shaded regions represent ±1σ standard deviation across events

7. Lines 302–312: The introduction and site description note that the locations are significantly influenced by sea–land breeze circulation. Although wind shifts are briefly mentioned for summer events, a more systematic analysis would be insightful. For example, could seasonal patterns in condensation sink (CS) and precursor delivery be partly explained by prevailing wind direction (marine vs. continental) and the strength of sea–land breezes in different seasons? A brief discussion explicitly linking the observed meteorological data (wind speed/direction) to seasonal NPF characteristics would add depth to the mechanistic analysis.

Response: We thank the reviewer for the constructive suggestion to provide a more systematic analysis linking air mass origins, sea-land breeze circulation, and seasonal variations in CS and precursor delivery. In response, we performed HYSPLIT backward

trajectory clustering (72 h, 1000 m) specifically for NPF days in each season. The results are now added in Section 3.3 (with supporting figures and tables in the Supplementary Material).

In summer, after NPF onset, the wind direction shifts sharply from northwesterly land breezes to northeasterly/easterly sea breezes. At 2 h, the frequency of marine winds surges to 50%, reaching 100% at 9 h. This wind shift reduces the CS to its seasonal minimum ($1.08 \pm 0.31 \times 10^{-2}\ s^{-1}$), creating a low-sink window that enables efficient growth. Subsequently, at +3 h, κ_{inorg} increases to 0.75 (matching marine CL3), confirming that the sea-land breeze is the primary physical trigger for summer NPF. In spring, unlike summer, the wind frequency in the NE/SE coastal sectors remains stable throughout the events, with marine/coastal air already accounting for 39.1% before NPF onset. This corresponds to CL2 (coastal pathway), which supplies a sustained high concentration of NH_3 ($6.76\ \mu g \cdot m^{-3}$), sufficient to overcome the high seasonal CS ($4.1 \times 10^{-2}\ s^{-1}$), leading to high particle formation efficiency. In winter, the large-scale northwesterly monsoon (CL1) dominates the background, carrying high BC ($1.86\ \mu g \cdot m^{-3}$). However, the air mass is never fully replaced; by +10 h, northwesterly winds return to 100%, and Cl 1 exhibits high κ_{inorg} (0.59), driving late-stage nitrate-dominated growth via cold condensation. In fall, Initial northwesterly winds (62.5% at -2 h) come from continental Cl 2 and 3, providing a favorable temperature (about 22 °C) and low CS. The subsequent southerly shift (44.4% at 2 h) introduces high-humidity air (RH > 71%), although the large-scale circulation remains dominated by continental air masses.

In summary, in spring and summer, NPF is significantly influenced by sea breezes (sea-land breeze replacement in summer, stable coastal transport in spring), which play a key role in reducing CS or supplying precursors. In fall and winter, although local winds occasionally blow from marine directions, the air-mass clustering analysis shows that the large-scale circulation is still governed by continental air masses, with local sea breezes playing only a limited modulating role.

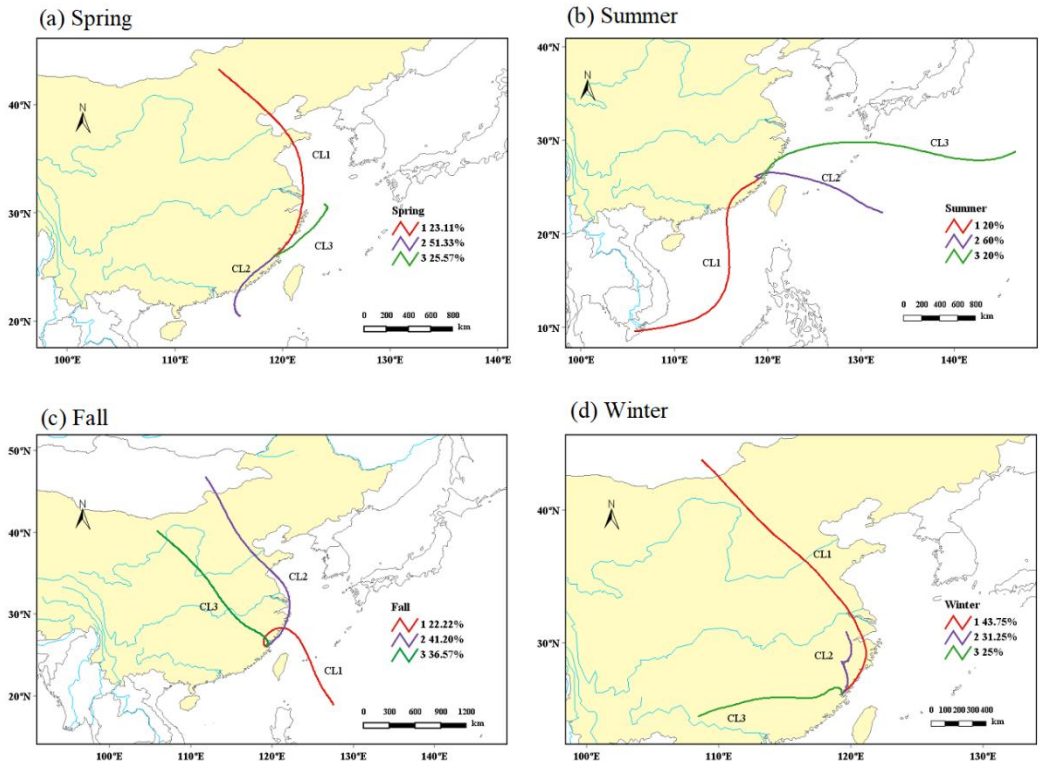

Fig.S8 Seasonal cluster analysis of 72-h back trajectories arriving at the Fuzhou site during NPF event days.

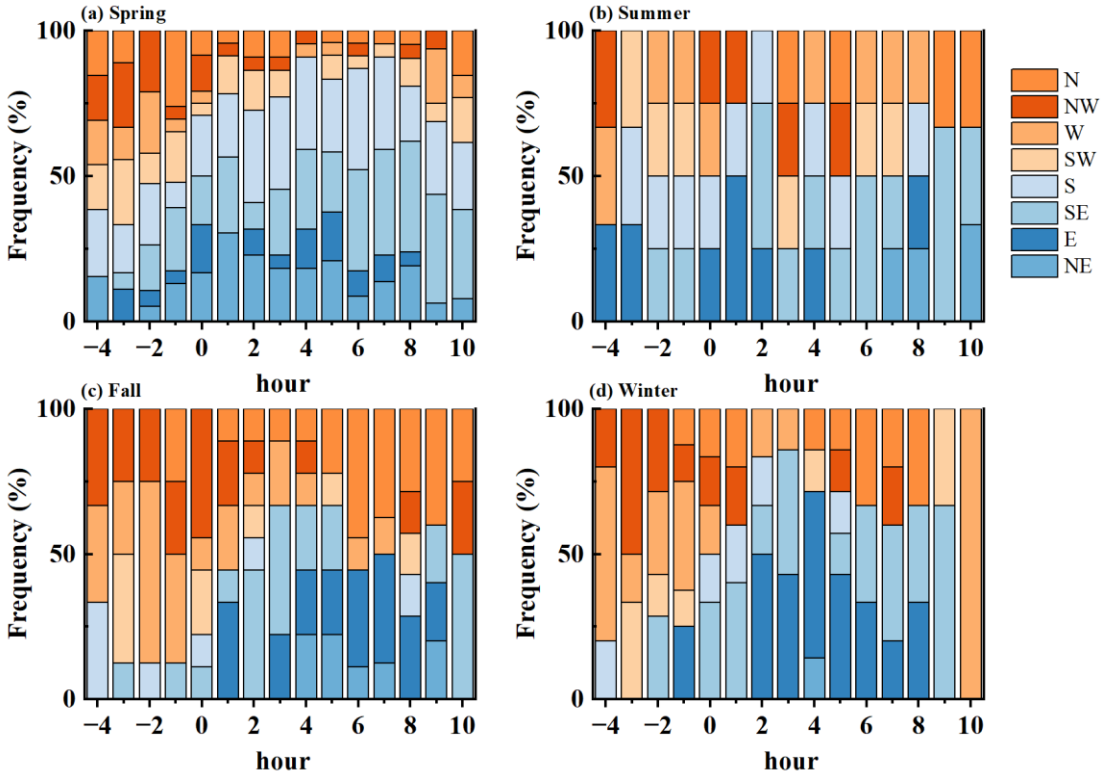

Fig.S9 Normalized diurnal frequency distribution of local wind directions surrounding NPF

onset (t=0 h) for different seasons. Time zero (0 h) marks the onset of the NPF event, with negative and positive values indicating hours before and after the onset. The eight wind sectors are color-coded, with warm colors representing continental origins and cool colors representing marine/coastal origins.

Table S3. Seasonal mean values (± standard deviation) of key NPF parameters (κ_{inorg}, Q, C, GR, CS, CoagS, and FR) for each trajectory cluster. The cluster proportion (%) is given in parentheses.

Season	Cluster (%)	κ_{inorg}	Q ($\times10^5$ $cm^{-3}\cdot s^{-}$)	C ($\times10^7$ cm^{-3})	GR ($nm\cdot h^{-}$)	CS ($\times10^{-2}$ s^{-})	CoagS ($\times10^{-4}$ s^{-})	FR ($cm^{-3}\cdot s^{-}$)
Spring	CL1 (23.11)	0.55±0.03	2.23±17.12	3.30±24.31	2.41±17.75	1.95±0.54	1.37±0.65	0.16±0.27
	CL2 (51.33)	0.52±0.03	0.39±15.65	0.68±12.70	0.50±9.27	4.36±2.14	5.61±4.00	6.65±9.92
	CL3 (25.57)	0.56±0.04	9.64±24.23	4.38±12.86	3.19±9.39	2.57±1.59	3.07±3.16	2.57±5.96
Summer	CL1 (20.00)	0.51±0.01	0.80±14.08	0.40±4.89	0.29±3.57	2.49±0.52	1.13±0.22	0.04±0.11
	CL2 (60.00)	0.55±0.03	3.63±34.62	0.98±10.31	0.71±7.52	1.08±0.31	1.01±0.65	0.06±0.24
	CL3 (20.00)	0.71±0.02	1.63±13.23	0.75±9.11	0.55±6.65	1.71±0.33	1.98±0.69	0.29±0.50
Fall	CL1 (22.22)	0.53±0.03	1.11±12.33	1.06±6.83	0.77±4.99	1.92±0.66	1.29±0.55	0.05±0.41
	CL2 (41.20)	0.58±0.05	2.45±15.34	0.90±7.37	0.65±5.38	1.70±0.71	1.18±0.75	0.08±0.25
	CL3 (36.57)	0.52±0.02	1.35±13.58	0.68±5.27	0.50±3.85	2.32±0.55	1.45±0.53	0.11±0.21
Winter	CL1 (43.75)	0.59±0.03	0.84±7.23	0.49±4.91	0.35±3.58	1.50±0.50	0.98±0.33	0.08±0.14
	CL2 (31.25)	0.58±0.04	0.07±6.75	-0.06±6.52	-0.05±4.76	2.15±0.56	1.06±0.49	0.07±0.20
	CL3 (25.00)	0.58±0.05	-1.41±9.38	-1.11±6.08	-0.81±4.44	2.50±1.02	1.32±0.52	0.07±0.16

Table S4. Seasonal mean values (±standard deviation) of precursor gas concentrations (HNO_3, HNO_2, HCl, NH_3, SO_2) for each trajectory cluster.

Season	Cluster (%)	HNO_3 ($\mu g\cdot m^{-3}$)	HNO_2 ($\mu g\cdot m^{-3}$)	HCl ($\mu g\cdot m^{-3}$)	NH_3 ($\mu g\cdot m^{-3}$)	SO_2 ($\mu g\cdot m^{-3}$)
Spring	CL1 (23.11)	0.57±0.03	0.58±0.26	0.06±0.06	1.26±0.53	1.27±1.10
	CL2 (51.33)	0.95±0.38	2.81±2.16	0.13±0.09	6.76±2.09	0.46±0.37
	CL3 (25.57)	0.66 ±0.14	1.38±1.39	0.09±0.06	4.00±1.76	0.71±0.48
Summer	CL1 (20.00)	1.22 ±0.36	1.92±1.26	0.25±0.12	7.44±1.26	0.62±0.33
	CL2	0.95±0.10	0.61±0.22	0.22±0.06	2.85±0.34	0.56±0.17

	(60.00)					
	CL3 (20.00)	0.93±0.07	0.49±0.08	0.23±0.05	2.98±0.24	0.53±0.07
	CL1 (22.22)	0.68±0.08	0.96±0.60	0.10±0.07	3.13±0.68	0.59±0.34
Fall	CL2 (41.20)	0.48±0.06	0.70±0.54	0.07±0.04	2.09±1.16	0.71±0.51
	CL3 (36.57)	0.50±0.08	1.08±0.87	0.06±0.02	2.59±0.57	0.83±0.32
	CL1 (43.75)	0.49±0.05	0.81±0.37	0.08±0.06	3.24±1.20	1.15±0.69
Winter	CL2 (31.25)	0.57±0.08	1.22±0.68	0.08±0.04	3.59±1.13	1.22±0.88
	CL3 (25.00)	0.58±0.09	2.36±2.83	0.07±0.04	3.83±2.73	0.92±0.64

8. Temperature and humidity effects: The text notes that high summer temperatures (>32°C) may inhibit nucleation (line 303), while lower fall temperatures (~22°C) appear favorable (lines 314–315). High relative humidity (RH >71%) in fall is also suggested to promote nucleation, likely by enhancing the uptake and hydration of sulfuric acid, a key nucleating precursor. These are valuable observations. Could the authors briefly expand the discussion, perhaps in a dedicated paragraph, to better quantify the impacts of temperature and RH? Specifically, elaborating on how temperature concurrently influences nucleation (FR) and condensable vapor production (affecting GR), and how RH modulates both initial nucleation probability and the subsequent CCN activation efficiency of grown particles, would provide a more complete picture of meteorological controls on the NPF–CCN lifecycle.

Response: We thank the reviewer for the valuable suggestion to quantify the impacts of temperature and RH on the NPF–CCN lifecycle. In response, we conducted an interpretable machine learning analysis using XGBoost (Extreme Gradient Boosting) combined with SHAP. The XGBoost model was trained to predict the observed nucleation rate (FR, 1.5–3nm particles) from multiple predictors, including temperature (T), RH, condensation sink (CS), and precursor gases (NH3, SO2). SHAP then attributes the model's output to each feature on a per-prediction basis, allowing us to extract nonlinear thresholds and interaction strengths directly from field data without assuming a predefined functional form. This approach is increasingly used in

atmospheric science to disentangle complex, interacting drivers.

The SHAP dependence plot for temperature reveals a unimodal, bell-shaped response: FR receives the strongest positive contribution in the 20–25°C range (SHAP ≈ +0.01), with contributions turning negative below 18 °C and above 28 °C, and strong suppression above 32°C (SHAP decreases by ~40% relative to the peak). This reflects a thermodynamic trade-off: moderate fall temperatures (22 °C) reduce the evaporation rate of H_2SO_4–NH_3 clusters, enhancing net FR, whereas summer heat (>32 °C) increases cluster volatility and inhibits nucleation. For the subsequent growth rate (GR) to CCN-active sizes, higher temperatures (25–30 °C) can enhance the production of condensable vapors (e.g., oxygenated organics), which may increase GR even as FR declines. We have explicitly discussed this trade-off in the revised manuscript. Regarding RH, contrary to the initial suggestion that high RH (>71%) promotes nucleation, our SHAP analysis shows a predominantly monotonic negative contribution of RH to FR (SHAP decreasing from +0.2 at RH≈50% to –0.6 at RH>71%). The apparent high-RH–high-FR correlation in fall is likely due to covariation with lower T and lower CS. Mechanistically, high RH suppresses nucleation via (i) reduced photolytic H_2SO_4 production under increased cloud cover, and (ii) enhanced CS from hygroscopic growth of pre-existing particles. However, once particles grow to ~30–50 nm, high RH strongly improves their CCN activation efficiency (Köhler theory). This dichotomous role of RH — suppressing nucleation but promoting activation — is now articulated in a dedicated paragraph, and we identify an optimal balance for net NPF–CCN yield at 50–65% RH combined with 20–25 °C.

Although the reviewer focused on T and RH, our SHAP analysis also yielded a novel, site-specific finding regarding precursor gases, which we have added to complement the meteorological discussion. NH_3 contributes approximately 2.1 times more to FR than SO_2 (1.3% vs. 0.6% of explained variance), and exhibits a sharp threshold at 4 μg m^{-3}. Below this value, NH_3 suppresses nucleation (SHAP negative); above it, the SHAP contribution turns positive and rises steeply (+0.2 at 10 μg·m^{-3}). This

quantitatively identifies Fuzhou as an NH_3-limited nucleation regime. All of the above quantitative results are now presented in a new subsection (Section 3.4) with two new figures (SHAP dependence plots for T, RH, and NH_3; interaction matrix).

Section 3.4:

3.4 Attribution analysis of particle formation and growth

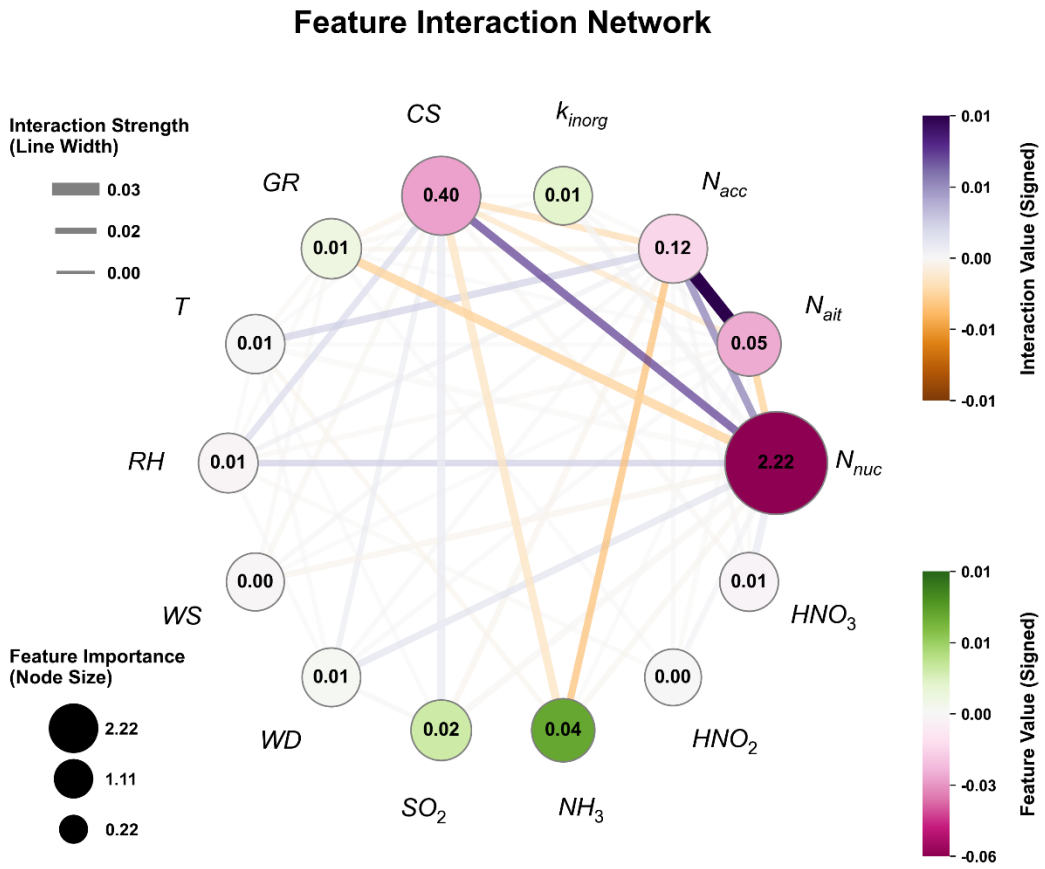

Fig. 2 Non-linear response relationships and interaction analysis between core environmental factors and FR. Node size and inner numbers denote feature importance (mean |SHAP|). Node color indicates contribution direction (green: positive; pink: negative). Edge width reflects interaction strength; edge color indicates interaction direction (purple: synergistic; orange: antagonistic).

According to SHAP analysis (Fig.S14), the main contributors to FR in Fuzhou are nucleation mode (76.2%), CS (13.8%), NH_3 (1.3%), and SO_2 (0.6%). Physical processes explain ~90% of the variance. A prominent feature is the sharp NH_3 threshold

at 4 μg·m^{-3}: below this, SHAP ≈ -0.025; above, it turns positive and rises by 0.2 at 10 μg·m^{-3}. CS shows a clear inhibition onset at 0.03 s^{-1}, with SHAP dropping from 0 to -0.5 as CS increases to 0.08 s^{-1}. Temperature has a positive SHAP only within 20–25°C (peak ~0.01), decreasing by 40% at 35°C. As shown in Fig. 7, the strongest interaction is between nucleation mode and CS (0.40), far exceeding other pairs (NH_3-nucleation mode: 0.04), highlighting that the net FR is governed by the competition between particle formation and scavenging.

For the Aitken mode, the driving forces shift notably. CS remains the top contributor, followed by accumulation mode (13.8%) and nucleation mode (7.1%). As shown in Fig.S15, a key distinction from FR is the temperature response. Instead of a bell shape, SHAP increases linearly from 0 to 0.1 over 20–35°C, indicating that high temperatures accelerate particle growth, enabling a rapid transition from nucleation to the Aitken mode. The NH_3 threshold at 4 μg·m^{-3} persists, showing its continued role in particle growth. RH exerts a linear negative effect, turning SHAP negative above 60%, suggesting hygroscopic growth or coagulation loss. In Fig.S16, the CS–nucleation mode interaction strength is 0.12, lower than in FR but still dominant, implying that strong nucleation can offset high CS losses.

In summary, the SHAP attribution reveals two distinct regimes. FR is dominated by CS, accompanied by a sharp chemical trigger (NH_3 >4 μg·m^{-3}) and a narrow temperature window (20–25°C). The Aitken mode, while still influenced by CS, is primarily driven by temperature-accelerated growth (linearly increasing above 20°C). Ammonia acts as a persistent enhancer in both stages, whereas high RH (>60%) consistently suppresses Aitken mode concentrations.

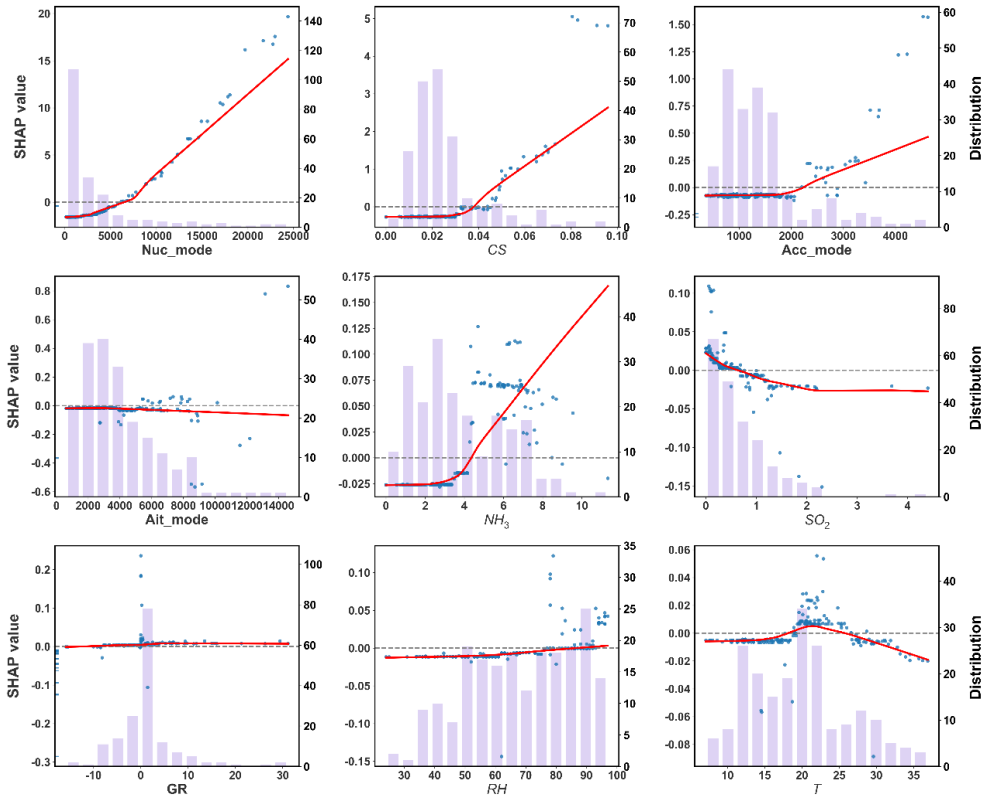

Fig.S14 Global importance analysis of influencing factors for particle formation rate (FR) based on SHAP summary plot.

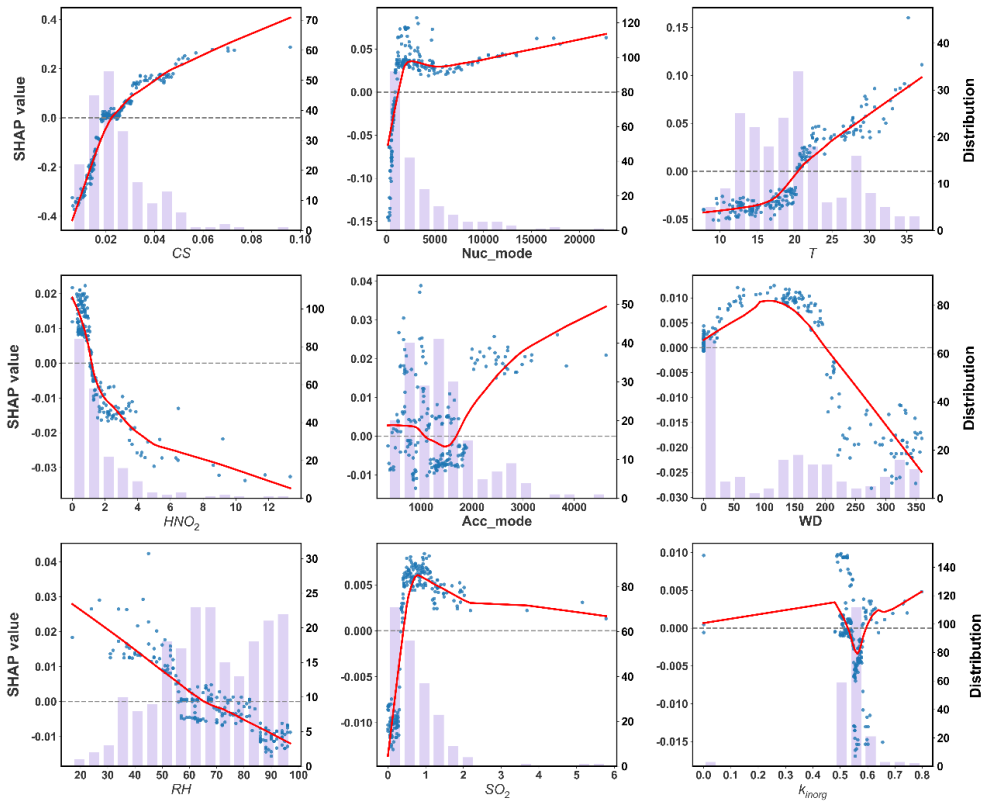

Fig.S15 Global importance analysis of influencing factors for N_{ait} based on SHAP summary plot.

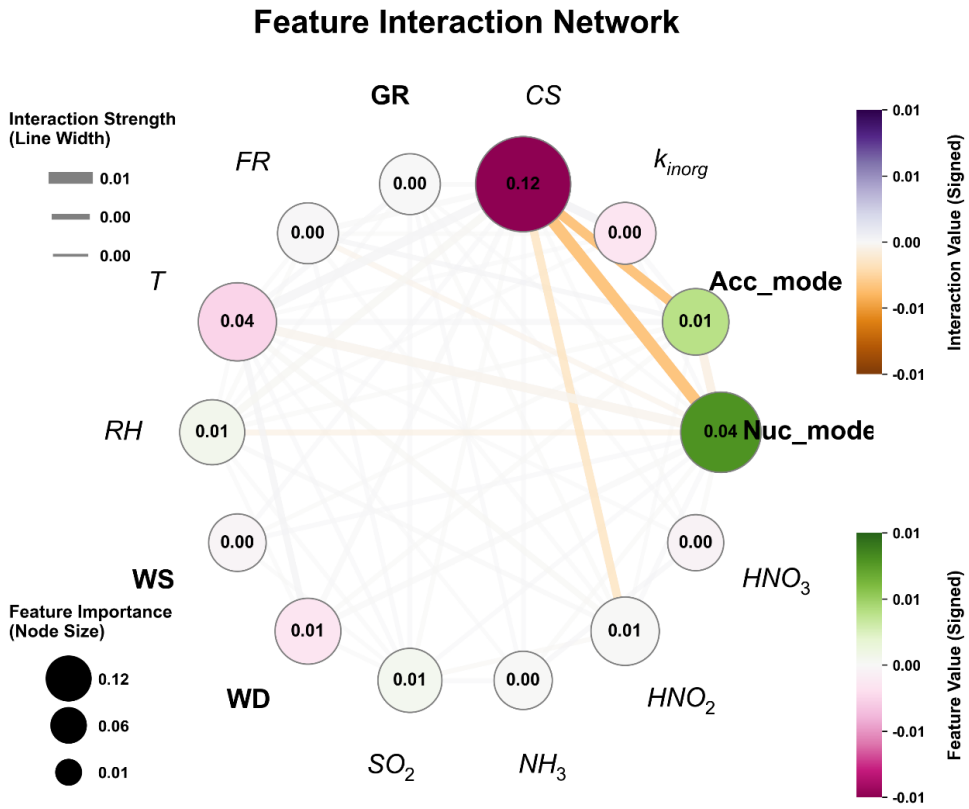

Fig.S16 Non-linear response relationships and interaction analysis between core environmental factors and N_{ait}.